Journal of
Materials Chemistry C

Accepted Manuscript

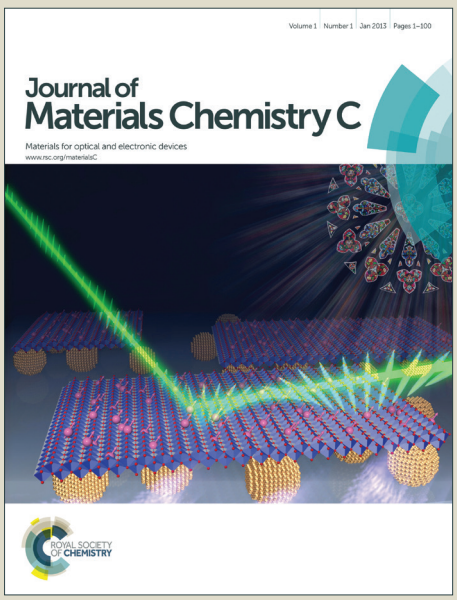

ROYAL SOCIETY OF CHEMISTRY

www.rsc.org/materialsC

Journal of Materials Chemistry C RSCPublishing

ARTICLE

Photorefractive performances of a graphene-doped PATPD/7-DCST/ECZ composite †

Cite this:

DOI: 10.1039/x0xx00000x

Received 00th January 2012,
Accepted 00th January 2012

DOI: 10.1039/x0xx00000x

www.rsc.org/

Panit Chantharasupawong[a], Cory W.Christenson[b], Reji Philip[a], , Lei Zhai[a], Jeffrey Winiarz[c], Michiharu Yamamoto[d] , Laurene Tetard[a*], Rahul R. Nair[e], Jayan Thomas[a*]

Photorefractive polymer composites have gained considerable attention due to their fascinating applications like 3D displays and 3D Telepresence. In this report, the performance of a novel PR polymer composite doped with graphene is studied. The addition of graphene laminates to a photorefractive composite results in up to threefold enhancement of space charge (SC) field build-up time. From our optical and electrical measurements, the faster build-up time is attributed to larger charge generation resulting from electronic interaction between graphene and the 7-DCST chromophores.

1. Introduction

Photorefractive (PR) polymer composites have gained considerable attention due to their advantages like large PR effect, structural flexibility, low cost and good processability compared to inorganic crystals. Since large diffraction efficiency can be obtained in a PR polymer composite sample that is several micrometers thick (as opposed to a few centimeters thick in the case of inorganic crystals), they are an interesting choice for large area and compact applications. Recently, remarkable advances have been accomplished in refreshable, eye-glass-free holographic three dimensional (3D) displays and 3D Telepresence using PR polymers [1-3]. Currently, there is a clear understanding of the physical phenomena taking place in PR polymers and the focus is to develop highly sensitive polymers for fast refreshing holographic 3D displays and 3D Telepresence [4, 5]. However, PR polymers currently available are not adequately sensitive to record holograms with low light intensity within a short exposure time. For instance, in order to achieve a sub-millisecond response time, a nanosecond (ns) pulsed laser with intensity as high as 4MW/cm^2 was required[6]. The sensitivity of PR polymers is therefore limited by the charge generation and separation efficiency.

The writing speed of the PR materials depends on two major factors: (1) formation of the space charge field ie. charge generation, transfer, transport and trapping; and (2) the reorientation dynamics of the chromophores. It is generally accepted that the former contributes to the fast time constant of the PR composite and the latter governs the slow time constant[7, 8]. Even though the limiting time factor for reaching the steady state in the PR polymers is the slow time constant, diffraction efficiencies smaller than the steady state diffraction value are sufficient for most practical dynamic holographic applications. For instance, an updatable hologram that can be viewed under ambient light condition with only 0.5% diffraction efficiency was recently demonstrated [9]. As a result, charge generation plays an important role in improving the temporal dynamics of hologram generation. It was found that, using proper charge generation moieties or sensitizers, like buckminister fullerene (C_{60}) or tetranitroflurinone (TNF), can substantially improve the writing dynamics of PR polymers[10, 11].

As a result, C_{60} has become one of the most commonly used,well-performing sensitizers in PR composites[12] and a benchmark sensitizer in the literature[15-18]. A more soluble derivative of C_{60}, [6,6]-phenyl C 61 -butyric acid methyl ester (PCBM) [13, 14], has also been used recently providing similar PR performance and easier material processing. However, while carbon nano-materials, particularly C_{60} and its derivatives, have proven to be efficient charge generators in PR composites, other carbon nano-materials within the same family of carbon allotropes, like single wall carbon nanotubes (CNTs) and multiwall carbon nanotubes, can also enhance the performance of PR composites[19-22]. Phase separation constitutes one of the processing challenges when dealing with CNT sensitizers. Recently, Lingam et al. [23] have bonded PVK polymer to CNTs. It was found that the charge-transfer process was improved through the intimate contact between the sensitizer and CTP. This grafted polymer system (PVK/7-DCST/TCP/PVK grafted CNT) showed internal diffraction efficiency as high as ~60% and two beam coupling gain of ~78 cm^{-1} at 633nm. Furthermore, CNTs are involved not only in the charge generation but also in charge transport,

which can occur along the tube. The photoconductivity of polymer composites with CNT was found to increase significantly compared to composites without CNTs[24, 25].

Carbon nanomaterials can be categorized by their dimensionality, which ranges from zero (0D) to 3D dimensions. One can think of the 2D configuration of carbon, namely graphene, as a building block to form the other dimensional structures of carbon allotropes such as 0D fullerene, 1D CNT, and 3D graphite. Graphene is a monolayer of carbon atoms densely packed into a two-dimensional honeycomb lattice, which can be regarded as a parent to C_{60} and CNTs, as it can be wrapped up to form 0D fullerene, rolled to form 1D CNT, and stacked to form 3D graphite[26]. Moreover, it is an interesting material with excellent electrical properties, mechanical flexibility, optical transparency, thermal conductivity, low thermal expansion coefficient and electronic properties[27-31]. Unlike semiconductors, the valence and conduction bands of graphene intersect at the Dirac point, indicative of a metallic like behavior with no energy band gap. Therefore, graphene can absorb and convert light into photocurrent over a broad electromagnetic spectral range, leading to great interest for its use in development of new optoelectronic materials. Under an applied electric field, photocurrent generation in graphene can occur under several processes such as Seebeck effect, photovoltaic effect, and bolometric effect[32, 33]. It has been found that electrical conductivity and photo-charge transport of polymer composites are improved with graphene doping[34-38]. Therefore, it is highly interesting to investigate the effect of graphene on the speed of grating formation in PR composites since the process involves both charge generation and transport.

Recently, Grishina et al. reported on the beam coupling properties of poly(N-vinylcarbazole)/ graphene composites at visible and infrared wavelengths[39, 40]. Neither plasticizers nor NLO chromophores were added in their system. The two beam coupling gain of the system was measured to be 50 cm^{-1} at an applied field of 150 V/μm and wavelength of 532 nm. However, such composite does not represent a real PR sample since it lacks NLO chromophore which is necessary for a PR system. Nevertheless, it is highly interesting to examine the use of graphene in a real PR polymer composite.

In this report, we studied the performance of a novel PR polymer composite doped with graphene at 633 nm. The system under study is composed of poly (acrylic tetraphenyldiaminobiphenyl) (PATPD) as the conducting polymer, N-ethyl carbazole (ECZ) as the plasticizer and 4-homopiperidinobenzylidenemalononitrile (7-DCST) as the NLO chromophore. We found that by adding graphene to the composite, photoconductivity and grating formation speed can be improved. We attribute such improvement to more efficient charge generation with graphene and donor-acceptor interaction between the graphene and the nonlinear chromophore.

2. Results and discussion

2.1 Effect of graphene on optical absorption of the PR composite

We prepared three PR samples by melt compounding process [see Experimental section for details]. The first sample (”undoped”) is an undoped sample consisting of PATPD/ECZ/7-DCST with 49.74/15.08/35.18wt%. The second sample (”graphene doped”) is graphene doped and the loading of graphene is about 0.03 wt% (graphene doped to ”undoped”). The third sample (”PCBM doped”) is a PR composite doped with the same wt% (0.03) loading of a benchmark PR sensitizer, PCBM for comparison. PCBM is selected as a standard sample for comparison here, since recent novel applications like updatable photorefractive 3D displays and 3D telepresence were demonstrated using samples sensitized with PCBM[9], although at different concentration. In the present work, we study the performance of a system similar to the one discussed in Reference 9 but using graphene additives. Since our graphene is not functionalized, maximum loading of 0.03% was used in our study to avoid graphene agglomeration. It is however important to note that the amount and performance of the PCBM in the present work are not comparable to that of Reference 9. In fact, decrease in rise time would be expected for higher weight percent, due to the subsequent larger number of photogenerated charges. All samples were prepared by sandwiching the PR composite between two indium tin oxide (ITO) coated glass slides with a controlled thickness of 105μm using spacers. Optical absorption spectra of these samples are shown in Figure 1(a). All samples show large absorption in the green region of the spectra. These large green absorptions are due to chromophore absorption. In order for PR effects to take place, light absorption is essential: this means that all PR samples will work well in the green region. However, since the light absorption is small in the red region, the addition of the sensitizers to the system is necessary. While the undoped and PCBM doped have similar absorption spectra, the graphene doped sample shows a longer absorption tail at longer wavelengths. The optical absorption of graphene dispersed in tetrahydrofuran (THF) shown in the inset of Figure 1(a) is in agreement with previous reports[41]. Therefore, improvement in the PR performances in the red region with the addition of graphene is expected. Comparing absorption spectra of the PR samples with their individual components, we found that the observed absorption profiles cannot be accounted for by simple superposition of the absorptions of the individual components. We have also measured absorption spectra of both undoped and graphene-doped composites without chromophores (Figure 1(b)). Both samples have high absorption at ~400 nm due to absorption of the polymers. The graphene-doped sample, however, exhibits higher residual absorption throughout the visible range. This higher residual absorption can be attributed to frequency-independent

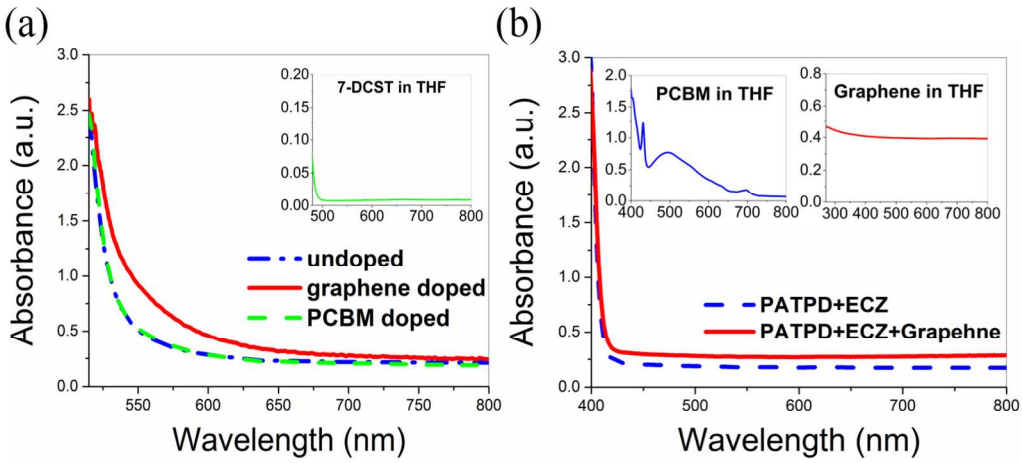

Figure 1 (a) Absorption spectra of undoped, graphene doped and PCBM doped in the film form. The inset shows the absorption of concentrated 7-DCST in THF. (b) Absorption of PR composites without chromophores (film) with (red) and without (blue) sensitizer. The addition of graphene results in broadband flat absorption in the visible wavelength range. The inset shows absorption of PCBM and graphene in THF. Axis labels of the insets are the same as of the main curves.

absorption of graphene[29, 42]. The existence of an absorption shoulder, only when chromophores are present in the graphene doped composite, suggests an interaction between the chromophores and graphene.

2.2 Studies on photorefractive performances of the graphene-doped PR composite

To measure the speed of refractive index grating formation in the PR process, we performed a transient four-wave-mixing (FWM) experiment. The wavelength used was 633 nm generated from a HeNe laser. It is to be noted that, in all of our experiments, the samples are pre-illuminated to avoid a history-dependent effect [43, 44]. In a typical FWM experiment, two coherent writing beams interfere inside the sample, resulting in an intensity modulation. This modulated intensity generates photo-generated charges which then drift and diffuse to form a space-charge (SC) field. The resulting SC field modulates the refractive index by electro-optic and reorientational effects, creating an index grating inside the material. To probe the formation dynamics of such gratings, another counter propagating beam or reading beam is used. Due to the index grating, the reading beam is diffracted and the transient behavior of the grating formation can be probed. The diffraction efficiency of this transmission grating depends on the strength of the grating according to the equation:

$$\eta \propto \sin^2(S) \qquad (1)$$

where S is the grating strength given by :

$$S = \frac{\pi \Delta n d}{\lambda \sqrt{\cos\alpha_1 \cos\alpha_2}} \cos(\alpha_1 - \alpha_2) \qquad (2)$$

with Δn being the magnitude of the index modulation, λ is the wavelength of the reading beam, and α_1 and α_2 are the angles of the writing beams with respect to the sample normal. Due to small dielectric screening in PR polymer, an external field is applied to facilitate charge separation and the sample is tilted to project an effective electric field along the grating vector. As a result, in the case of PR polymers, Δn is a function of applied field and SC-field dependent birefringence and the electro-optic effect of the chromophore. Since the generation of SC-field and thus the index grating are dynamic in nature, Δn is a function of both time and voltage. In transient FWM measurements, we monitored the temporal behavior of the diffracted beam at a constant applied field of 64 V/μm as one of the writing beams is blocked and then opened. The total writing intensity used was 800 mW/cm^2. From these measurements, shown in Figure 2(a), we found that the graphene doped sample showed faster dynamics than the other samples. Such observation indicates a faster formation of the refractive index grating. We have also measured the steady-state FWM properties of the samples [Supporting information, FigureS1]. All three samples showed comparable diffraction efficiency. At the applied field of 64V/μm, the undoped, graphene doped and PCBM doped samples have internal diffraction efficiency of 69%, 62%, and 53% respectively.

In general, the speed of the formation of the index grating depends on two contributions, (1) speed of SC-field formation and (2) chromophore reorientation time. The first contribution is largely affected by the charge generation efficiency of the sensitizers while the second contribution depends on the properties of the chromophore and the T_g of the composite. In fitting the transient data, the assumption of bi-exponential character in the transient behavior of the index modulation, $\Delta n(t)$, results in two time constant, i.e. the fast

time constant t_1 and the slow time constant t_2, as seen in Equation (3).

$$\Delta n(t) \propto [1 - m\exp(-t/t_1) - (1-m)\exp(-t/t_2)] \quad (3)$$

Since the SC-field formation is much faster than the reorientation of the chromophores, t_1 can be mainly attributed to the speed of the SC-field formation. On the other hand, t_2 mostly reflects the chromophore reorientation kinetics[7]. By fitting our data with Equation (3), t_1 and t_2, for graphene doped are determined to be 0.8 s and 25 s respectively. In contrast, for undoped, t_1 = 2.5 s and t_2 = 25s, and for PCBM doped t_1 = 1.8 s and t_2 = 38 s. The weighting factor m used for fitting undoped, graphene doped and PCBM doped data are 0.51, 0.51, and 0.65s respectively. When compared to its undoped counterpart, the graphene doped sample has approximately 3 times faster t_1 while their t_2 values are the same. Such reduction in the fast time constant, i.e. the faster SC-field formation can be attributed to the improved charge generation and transport due to the presence of graphene. In order to verify this assumption, we performed photoconductivity measurements (Figure 2(b)). The total light intensity used for all measurements was 400mW/cm^2. The speed of the SC-field formation and the value of the magnitude of the t_1 value are largely governed by the photogeneration efficiency. We found that our graphene-doped sample exhibits significantly larger photoconductivity, σ_{ph}, than the undoped sample. Its photoconductivity also is larger than that of PCBM-doped sample when applied filed is larger than 30V/μm. This larger photoconductivity in the graphene-doped sample means, given the same irradiation, more charges (larger photocurrent) are generated in the sample. By the definition of electric current, a larger current is the manifestation of a greater number of charges flowing through the sample per time interval. In the case of the PR polymer, this enhanced charge flow will result in a faster formation of a steady state SC-field. Therefore, the observed largest photoconductivity in the graphene-doped sample explains its fastest t_1. We also calculated the photo-charge generation efficiency, ϕ_{ph}, of the samples according to the equation

$$\varphi_{ph} = \frac{\sigma_{ph} E h v}{e I_a} \quad (4)$$

where E is the applied electric field, I_a is the absorbed light intensity, h is Planck's constant, v is the light frequency, and e is the elemental charge constant. It is found that the photogeneration efficiencies of all samples increase with E, as depicted in Figure 2(c). Such field dependent efficiency suggests the electric field assisted dissociation of excitons [45, 46]. In other words, holes and electrons are generated at the interface between two species (donor and acceptor). From the experimental data, the rate of increase of the efficiency with applied field is higher in the case of the graphene-doped sample compared to that of the undoped sample. This higher rate is an indication of a smaller initial electron-hole separation, or exciton thermalization length, in the graphene-doped sample[47]. Such reduction in the initial thermalization length may be explained by the small loading of the graphene. The number of participating charge generators can

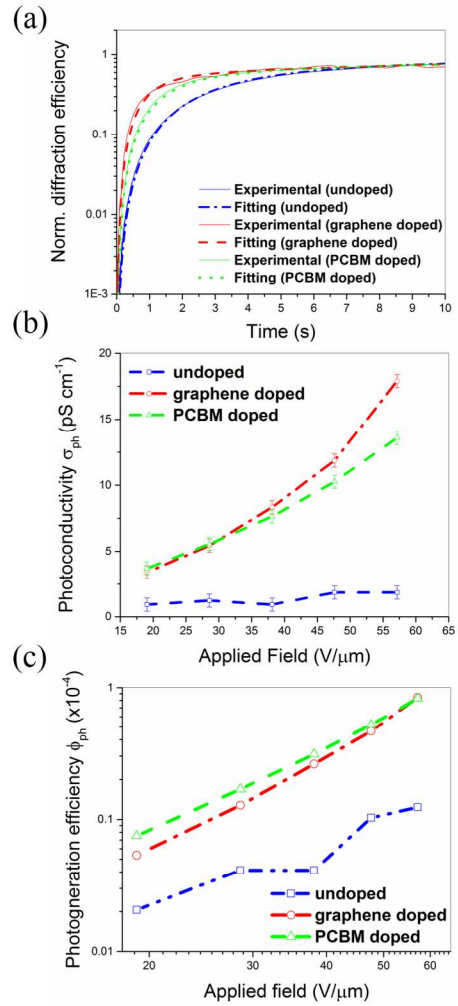

Figure 2 (a) Transient FWM curves (b) Photoconductivity vs. applied field and (c) Photo-charge generation efficiency of undoped, graphene doped, and PCBM doped.

significantly affect the interfacial area between donor and acceptor species and the thermalization length is highly dependent upon the interfacial areas[48]. Larger loadings of both species can result in continuous pathways available to both electrons and holes and thus a longer thermalization length. On the other hand, the absence of such pathways in either one of the charge species causes a reduction in the thermalization length. The undoped sample has a large initial thermalization length (smaller slope) because the charge generation and separation occurs between two species with large loadings which are, in this case, the chromophores and the charge transporting polymers. From the experiments, we found that the graphene-doped sample had much larger

photo-charge generation than its undoped counterpart. It becomes obvious that the additional charges are generated by the presence of graphene. The observed reduction in the initial thermalization length in the graphene-doped sample further confirms that such increase in photogeneration involves the species with smaller loading, i.e. graphene.

Since any species added to the PR polymer composites can also act as charge traps[49, 50], it is interesting to investigate this aspect. We performed two beam coupling (TBC) measurements with our sample (Figure 3). In this experiment, the energy exchange between two overlapping laser beams was monitored. The magnitude of the energy exchange is expressed in the form of the gain coefficient, Γ, which depends not only on the magnitude of the SC-field but also on the phase shift between the light interference pattern and the index modulation[51]. Charge trapping can affect both the magnitude and the phase of the SC-field, resulting in changes in the magnitude of Γ[52]. Not only that, TBC measurement implicitly gives information about the trapping mechanisms, the non-zero TBC gain coefficient is a proof of the PR effect in the system due to the nonlocal nature of the PR effect. We found that the gain coefficients of our graphene-doped sample are comparable to those of the undoped sample. This observation indicates that the addition of graphene neither affect the magnitude nor the phase of the SC-field, possibly due to the absence of new favorable charge traps (otherwise, very shallow traps) generated with graphene. Both samples showed large gains with p-polarized beams. This is because the index modulation seen by p-polarized light is stronger than by s-polarized light. It is to be noted here that both samples showed reversed direction of energy transfer as the incident beams were changed from s-polarization to p-polarization. This effect has previously been observed[53].

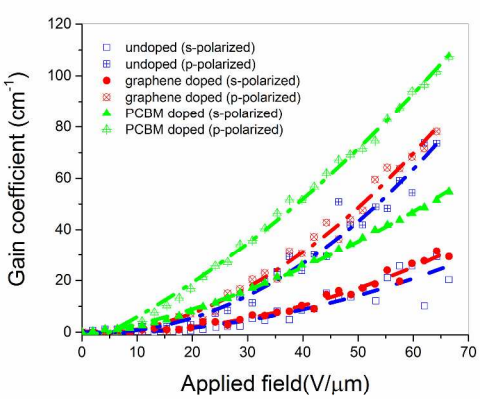

Figure 3 Γ vs. E for undoped, graphene doped and PCBM doped. Data for both s- and p-polarizations are shown.

When the performance of the graphene-doped sample was compared with a PR polymer doped with the benchmark sensitizes, like in the PCBM doped, we found that t_1 of the graphene-doped sample is shorter than that of the PCBM-doped sample at an applied voltage of 64V/μm. The shorter time constant in this graphene-doped sample is in accordance with its higher photoconductivity when compared to the PCBM-doped sample. However, the linear absorption of the graphene-doped sample is higher than that of the PCBM-doped sample at similar loading levels. The rate of increase in the photocharge generation efficiency of the graphene-doped sample, however, is larger than that of the PCBM-doped sample. We also found that the TBC gain coefficient is much higher in the case of the PCBM-doped sample. The larger TBC gain in the PCBM-doped sample can be attributed to traps generated from ionized sensitizers [54]. In the PCBM system, the majority of charges are generated from photoexcitation of PCBM molecules. By transferring holes to the transport polymer, ionized PCBMs are created. These species act as electron traps that increase the separation between positive and negative charges, resulting in large TBC gain. On the other hand, graphene-doped sample and undoped sample have similar gain coefficients, suggesting the lack of such trapping mechanism. This implicates that charge sensitization processes in PCBM-doped and graphene-doped samples are different. In the former, PCBM acts as independent charge sensitizers and ionized species are the results of photoexcitation. In the latter, however, graphene helps separation and transport of charges created from photoexcitation of the nonlinear chromophores as evident by photocurrent, absorption and PL measurements (discussed in the following section).

2.3 Effect of graphene on photoluminescence of the PR composite

From the TBC measurements, it is clear that the PR effect can take place in the PATPD/ECZ/7-DCST system, without the use of additional sensitizer, i.e. the case of the undoped sample. However, we found that the absorption profile of the composite is not a simple superposition of the component's profiles. This finding suggests electronic interactions between the components. To have an insight into this aspect, we performed photoluminescence (PL) measurements with 532

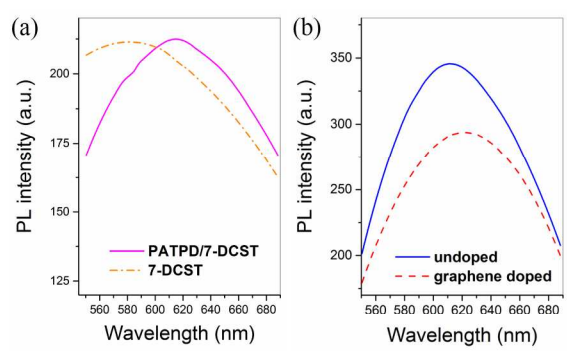

Figure 4. PL spectra of (a) PATPD/7-DCST composite and 7-DCST, and (b) graphene doped and undoped PR samples. The excitation wavelength was at 532nm. The composites studied here were so prepared that the % weight loading of the components in polymer matrices are the same as those of the PR samples.

nm laser excitation (Figure5) using a Raman confocal microscope (Witec Alpha 300 RA Raman system). First, we investigated the PL of the PATPD /7-DCST composite to observe the interaction between PATPD and 7-DCST. The PL of the PATPD/7-DCST composite has a peak at ~ 610 nm which is red-shifted compared with the PL of 7-DCST (Figure 4(a)). These results suggest that excited 7-DCST electronically interacts with the PATPD host polymer. The PL spectra of thin layers of undoped and graphene doped samples are shown in Figure 4(b). The undoped sample has a PL peak at 610 nm which is same as the PL peak of the PATPD/7-DCST composite. The observed peak at 610nm in the undoped PR composite may be attributed to the radiative recombination between electron in the LUMO level of 7DCST and hole in the HOMO level of PATPD as illustrated in Figure 5(a). However, according to our previous optical measurements, the photo-charge generation efficiency of this system is relatively small which results in a slow formation of the SC-field.

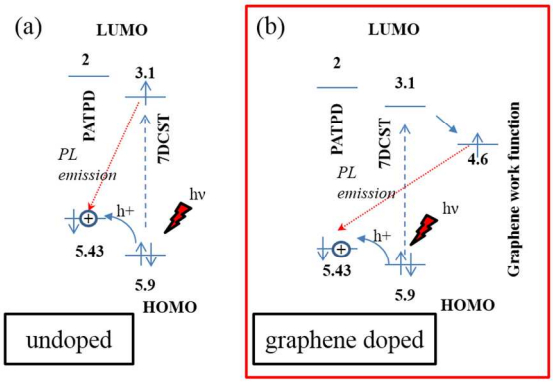

Figure 5 Possible charge interaction diagram for (a) undoped and (b) graphene doped. In the undoped PR composites, a photo-generated hole is transferred from 7-DCST to PATPD. ECZ does not participate in hole transport due to its lower HOMO level of 5.92eV. These holes are the primary charge conductors in PR polymers. In the case of graphene doped, graphene may act as an electron acceptor with 7-DCST as a donor, resulting in better exciton dissociation/charge generation efficiency.

By adding graphene to the system, the efficiency can be improved. This improvement in the efficiency results in faster formation of a SC-field and shorter t_1. Here, we found that graphene can be used to improve the photocharge generation efficiency of the PR system. Even without optimization and functionalization, the photo-charge generation efficiency of the graphene sensitizers is similar to benchmark materials like PCBM. We also found that the absorption of the graphene doped sample has a longer tail in the red region than those of the undoped and PCBM doped. The PL spectrum of the graphene doped PR is also slightly red-shifted compared to that of the undoped. Considering the energy level of graphene (Figure 5(b)), it is possible that graphene interacts electronically with the LUMO level of 7-DCST, resulting in the slight red-shift in the PL spectrum and better charge generation efficiency. In fact, electronic interactions between graphene and π-conjugated polymers has been observed in the case of photonic and optoelectronic devices[55-59]. It has also been found that electron transfer occurs between poly(3-octylthiophene) and graphene where graphene acts as an acceptor [57]. In addition, blending conjugated polymers with graphene-based materials can result in effective electron–hole separation and charge transport. It also provides a continuous pathway for charge transfer [59].

2.4 The role of charge trapping in the graphene-doped PR composite.

While both graphene-doped and PCBM-doped samples have similar charge generation efficiency, the latter shows much stronger TBC gain. This finding can be explained in terms of charge trapping in the composites. In the PCBM-doped system, the generated charges are transferred to the conducting polymer, resulting in ionized PCBMs. The ionized PCBMs act as hole traps. However, in the case of the graphene-doped sample, the presence of graphene in the system does not significantly affect the magnitude of the TBC gain, suggesting the lack of a trapping mechanism.

An increase in the speed of the SC-field formation can be the manifestation of two phenomena, namely more efficient photo-charge generation and better charge transport. Since we observed an increase in photo-charge generation efficiency, we conclude that better charge generation process due to the interaction between graphenes and the complex is responsible for the improvement. However, it is also possible that the addition of graphene helps transporting the photo-generated charges, possibly by improving overall electrical conductivity of the composite. Enhancement in electrical

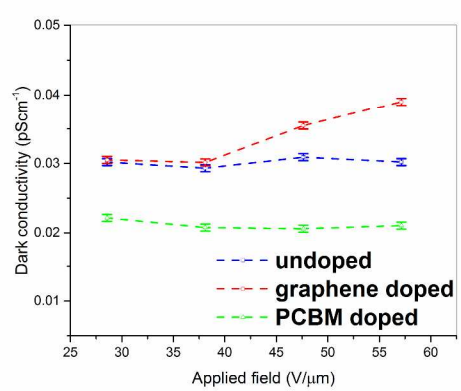

Figure 6 Dark conductivity vs applied field for undoped, graphene doped and PCBM doped.

conductivity of graphene-doped composites has been observed previously[60]. In order to investigate this aspect, we looked at the dark-conductivity of the samples (Figure 6). The dark conductivity was measured at the steady state after pre-illumination. We found that both undoped and graphene doped have similar dark-conductivity at low voltages. However, graphen doping showed slightly higher conductivity at larger fields. It is possible that the addition of graphene leads to such voltage dependent enhancement of the dark conductivity. This aspect is the subject of future study. However, we can conclude that, in our graphene–doped PR composite, the graphene dopants do not negatively affect the charge transport mechanism. In other words, charge trapping is absent in the graphene-doped sample. On the contrary, The PCBM doped shows a reduction in dark-conductivity when compared with the undoped. This can be attributed to the trapping mechanism previously discussed.

3. Experimental

3.1 Sample preparations

Graphene used in this experiment was synthesized by chemical exfoliation according to previous reports[61, 62]. Briefly, graphene samples were prepared by ultrasonic cleavage of high purity HOPG in an organic solvent, N-methylpyrrolidone. The resulting solutions were centrifuged to obtain a stable dispersion. This dispersion contains 10-50 nm graphene crystallites, predominantly mono and bilayers. These dispersions were filtered through alumina filters to obtain μm thick free standing graphene laminates. These graphene laminates were re-dispersed in THF to produce PR samples.

All samples were prepared by melt processing. First, the chemicals were mixed with the designated composition in a common solvent, THF. The solution was then dried at 55 °C under vacuum for 24hr. The mixture solid was placed between two indium-tin-oxide (ITO) and melt processed at 165 °C. Polystyrene glass beads of 105 μm diameter were used as a spacer to control the thickness of the samples.

3.2 Optical absorption measurement

The absorption spectra of all samples were taken using fiber-coupled light source (DH-2000) and spectrophotometer (USB4000) from Ocean Optics. The absorption coefficients at 633nm were determined and confirmed using a power meter (Newport 1918-R) equipped with a silicon photodiode (Newport 818-SL).

3.3 FWM measurement

In this measurement, two writing beams of equal intensities of 400mW/cm^2 were used. The wavelength was 633nm generated from a HeNe laser. The intensity of the reading beam was 21mW/cm^2. The tilt angle between the sample normal and bisect of the two writing beams was fixed at 55°. The angle between two writing beams was fixed at 24° for all measurements. Photodiodes connected to a digital oscilloscope were used to measure the transient behaviors. The transient measurements were done by blocking and un-blocking one of the writing beams using a mechanical shutter. The intensity of the diffracted beam was monitored once the shutter was open. The internal diffraction efficiencies, η_{int}, were calculated using the following equation:

$$\eta_{\text{int}} = \frac{I_{diff}}{I_{diff} + I_{trans}} \quad (5)$$

where I_{diff} and I_{trans} are the diffracted and transmitted intensities, respectively.

3.4 TBC measurement

In TBC measurements, two interacting beams with a 1:1 intensity ratio were used. The gain coefficients, Γ, for a sample with thickness, L, were calculated via the equation[15].

$$\Gamma = \frac{1}{L}[\ln(b\gamma) - \ln(b+1-\gamma)] \quad (6)$$

with the gain $\gamma = I_1(I_2 > 0)/I_1(I_2 = 0)$ and the intensity ratio b =1.

3.5 Photocurrent and dark-current measurements

In photocurrent measurement, the samples were irradiated with uniform laser beam (633nm) of 400mW/cm^2 and the photogenerated currents flowing through the samples were measured using a *Keithley 6485 picoampmeter*. The currents under dark conditions (dark-current) were also recorded. The photoconductivity, σ_{ph}, was calculated according to the following formula.

$$\sigma_{ph} = \frac{i_{tot}}{EA_{beam}} - \sigma_{dark}\left(\frac{A_{elec}}{A_{beam}} - 1\right) \quad (7)$$

where i_{tot} is the total current, σ_{dark} is the dark conductivity, E is the applied electric field, A_{elec} is the electrode area, and A_{beam} is the illumination area.

3.6 PL measurements

A confocal Raman system from Witec (Alph300RA) was used to acquire the photoluminescence spectra. The excitation light at 532 nm was focused using a 20X objective. The spectra presented in Figure 5 are the results of 5 accumulations single spectra with 0.5s integration time using

the 600 g/mm grating of the UHTS300 spectrometer centered at 620 nm.

Conclusions

In conclusion, we have studied the performance of PR composites doped with graphene. We found that, in the undoped system of PATPD/ECZ/7-DCST, charge sensitization occurs via nonlinear chromophores. Nonetheless, the addition of graphenes to the system results in shorter SC-field build-up time. The faster build-up time is attributed to larger charge generation due to the electronic interaction between graphenes and chromophores. Photocurrent studies on our samples confirm the enhancement in charge generation with the addition of graphene. From the energy levels of the component and our luminescence study, it is likely that the improved charge generation is due to the efficient exciton separation at the 7DCST-grapehne interface. The PR performance of the grapehene-doped sample are comparable with the PCBM-doped sample with the same (wt%) loading. We found that the graphene-doped sample exhibited faster SC-field build up time and larger photoconductivity at high applied field (>50V/μm). The steady state TBC gain of the sample doped with the benchmark sensitizer PCBM is larger than that of the graphene-doped PR composite. However, the TBC gains of the graphene-doped sample are comparable with the undoped composite. The absence of improvement in the TBC gains of the graphene-doped sample compared with PCBM-doped sample may be attributed to the lack of charge trapping in the graphene-doped sample. This study has revealed the potential of using graphene-based materials to improve the speed of PR polymer composites. Future work will focus on further enhancement of the PR speed by increasing the loading of graphene by suitable functionalization.

Acknowledgements

J.T acknowledges NSF CAREER award (ECCS-1351757) for the financial support.

Notes and references

[a] NanoScience Technology Center and College of Optics and Photonics, CREOL, University of Central Florida, Orlando, FL 32816, USA, Email: Laurene.Tetard@ucf.edu; Jayan.Thomas@ucf.edu.
[b]Department of Physics, Case Western Reserve University, Cleveland, OH 44106,USA
[c]Department of Chemistry, Missouri University of Science and Technology, Rolla, MO 65409-0010, USA
[d]Nitto Denko Technical Corporation, Oceanside, California 92054, USA.
[e]School of Physics and Astronomy, The University of Manchester, Manchester M13 9PL, UK
†Electronic Supplementary Information (ESI) available: [Steady state FWM]. See DOI: 10.1039/b000000x/

1. S. Tay, P. A. Blanche, R. Voorakaranam, A. V. Tunc, W. Lin, S. Rokutanda, T. Gu, D. Flores, P. Wang, G. Li, P. St Hilaire, J. Thomas, R. A. Norwood, M. Yamamoto and N. Peyghambarian, *Nature*, 2008, **451**, 694-698.
2. P. A. Blanche, A. Bablumian, R. Voorakaranam, C. Christenson, W. Lin, T. Gu, D. Flores, P. Wang, W. Y. Hsieh, M. Kathaperumal, B. Rachwal, O. Siddiqui, J. Thomas, R. A. Norwood, M. Yamamoto and N. Peyghambarian, *Nature*, 2010, **468**, 80-83.
3. J. Thomas, R. A. Norwood and N. Peyghambarian, *Journal of Materials Chemistry*, 2009, **19**, 7476-7489.
4. J. Thomas, C. W. Christenson, P.-A. Blanche, M. Yamamoto, R. A. Norwood and N. Peyghambarian, *Chemistry of Materials*, 2010, **23**, 416-429.
5. F. Gallego-Gomez, M. Salvador, S. Kober and K. Meerholz, *Applied Physics Letters*, 2007, **90**, 251113-251113.
6. M. Eralp, J. Thomas, S. Tay, G. Li, A. Schulzgen, R. A. Norwood, M. Yamamoto and N. Peyghambarian, *Applied Physics Letters*, 2006, **89**, 114105-114105-114103.
7. O. Ostroverkhova and K. D. Singer, *Journal of Applied Physics*, 2002, **92**, 1727-1743.
8. W. E. Moerner, S. M. Silence, F. Hache and G. C. Bjorklund, *J. Opt. Soc. Am. B*, 1994, **11**, 320-330.
9. P.-A. Blanche, A. Bablumian, R. Voorakaranam, C. Christenson, W. Lin, T. Gu, D. Flores, P. Wang, W.-Y. Hsieh and M. Kathaperumal, *Nature*, 2010, **468**, 80-83.
10. S. M. Silence, C. A. Walsh, J. C. Scott and W. E. Moerner, *Applied Physics Letters*, 1992, **61**, 2967-2969.
11. K. Meerholz, B. L. Volodin, Sandalphon, B. Kippelen and N. Peyghambarian, *Nature*, 1994, **371**, 497-500.
12. S. Köber, M. Salvador and K. Meerholz, *Advanced Materials*, 2011, **23**, 4725-4763.
13. E. Mecher, C. Brauchle, H. H. Horhold, J. C. Hummelen and K. Meerholz, *Physical Chemistry Chemical Physics*, 1999, **1**, 1749-1756.
14. S. Kober, F. Gallego-Gomez, M. Salvador, F. B. Kooistra, J. C. Hummelen, K. Aleman, S. Mansurova and K. Meerholz, *Journal of Materials Chemistry*, 2010, **20**, 6170-6175.
15. K. Ditte, W. Jiang, T. Schemme, C. Denz and Z. Wang, *Advanced Materials*, 2012, **24**, 2104-2108.
16. D. J. Binks, S. P. Bant, D. P. West, P. O'Brien and M. A. Malik, *Journal of Modern Optics*, 2003, **50**, 299-310.
17. X. Li, J. Van Embden, J. W. M. Chon, R. A. Evans and M. Gu, *Applied Physics Letters*, 2010, **96**, 253302-253302-253303.
18. F. Gallego-Gómez, J. A. Quintana, J. M. Villalvilla, M. a. A. Díaz-García, L. Martín-Gomis, F. Fernández-Lázaro and A. n. Sastre-Santos, *Chemistry of Materials*, 2009, **21**, 2714-2720.
19. A. V. Vannikov, R. W. Rychwalski, A. D. Grishina, L. Y. Pereshivko, T. V. Krivenko, V. V. Savel'ev and V. I. Zolotarevskii, *Opt. Spectrosc.*, 2005, **99**, 643-648.
20. A. D. Grishina, L. Y. Pereshivko, L. Licea-Jiménez, T. V. Krivenko, V. V. Savel'ev, R. W. Rychwalski and A. V. Vannikov, *High Energy Chem*, 2007, **41**, 267-273.

21. A. D. Grishina, L. Licea-Jimenez, L. Y. Pereshivko, T. V. Krivenko, V. V. Savel'ev, R. W. Rychwalski and A. V. Vannikov, *High Energy Chem*, 2006, **40**, 341-347.
22. L. Licea-Jiménez, A. D. Grishina, L. Y. Pereshivko, T. V. Krivenko, V. V. Savelyev, R. W. Rychwalski and A. V. Vannikov, *Carbon*, 2006, **44**, 113-120.
23. N. K. Lingam, S. Kalghatgi and J. G. Winiarz, *Journal of Applied Physics*, 2011, **109**, 023106-023110.
24. N. V. Kamanina, N. A. Shurpo, Y. A. Zubtsova, A. V. Prokhorenkov, S. V. Serov, P. Y. Vasilyev, V. I. Studeonov and F. Kajzar, 2010, 78381G-78381G.
25. L. Cao, H. Chen, M. Wang, J. Sun, X. Zhang and F. Kong, *The Journal of Physical Chemistry B*, 2002, **106**, 8971-8975.
26. A. K. Geim and K. S. Novoselov, *Nat Mater*, 2007, **6**, 183-191.
27. A. C. Neto, F. Guinea, N. Peres, K. S. Novoselov and A. K. Geim, *Reviews of modern physics*, 2009, **81**, 109.
28. C. Lee, X. Wei, J. W. Kysar and J. Hone, *Science*, 2008, **321**, 385-388.
29. R. R. Nair, P. Blake, A. N. Grigorenko, K. S. Novoselov, T. J. Booth, T. Stauber, N. M. R. Peres and A. K. Geim, *Science*, 2008, **320**, 1308.
30. S. Bae, H. Kim, Y. Lee, X. Xu, J.-S. Park, Y. Zheng, J. Balakrishnan, T. Lei, H. R. Kim and Y. I. Song, *Nature nanotechnology*, 2010, **5**, 574-578.
31. A. A. Balandin, *Nat Mater*, 2011, **10**, 569-581.
32. M. Freitag, T. Low, F. Xia and P. Avouris, *Nat Photon*, 2013, **7**, 53-59.
33. X. Xu, N. M. Gabor, J. S. Alden, A. M. van der Zande and P. L. McEuen, *Nano Letters*, 2009, **10**, 562-566.
34. S. Stankovich, D. A. Dikin, G. H. B. Dommett, K. M. Kohlhaas, E. J. Zimney, E. A. Stach, R. D. Piner, S. T. Nguyen and R. S. Ruoff, *Nature*, 2006, **442**, 282-286.
35. H. Pang, T. Chen, G. Zhang, B. Zeng and Z.-M. Li, *Materials Letters*, 2010, **64**, 2226-2229.
36. H. J. Salavagione, G. Martinez and M. A. Gomez, *Journal of Materials Chemistry*, 2009, **19**, 5027-5032.
37. N. Yang, J. Zhai, D. Wang, Y. Chen and L. Jiang, *ACS Nano*, 2010, **4**, 887-894.
38. P. V. Kamat, *The Journal of Physical Chemistry Letters*, 2011, **2**, 242-251.
39. A. D. Grishina, T. V. Krivenko, V. V. Savel'ev, R. W. Rychwalski and A. V. Vannikov, *High Energy Chem*, 2013, **47**, 46-52.
40. A. D. Grishina, T. V. Krivenko, V. V. Savel'ev, R. W. Rychwalski and A. V. Vannikov, *High Energy Chem*, 2013, **47**, 187-191.
41. V. G. Kravets, A. N. Grigorenko, R. R. Nair, P. Blake, S. Anissimova, K. S. Novoselov and A. K. Geim, *Physical Review B*, 2010, **81**, 155413.
42. K. F. Mak, M. Y. Sfeir, Y. Wu, C. H. Lui, J. A. Misewich and T. F. Heinz, *Physical Review Letters*, 2008, **101**, 196405.
43. A. Grunnet-Jepsen, D. Wright, B. Smith, M. Bratcher, M. DeClue, J. Siegel and W. Moerner, *Chemical physics letters*, 1998, **291**, 553-561.
44. H. Bolink, V. Krasnikov, G. Malliaras and G. Hadziioannou, *The Journal of Physical Chemistry*, 1996, **100**, 16356-16360.
45. R. H. Batt, C. L. Braun and J. F. Hornig, *The Journal of Chemical Physics*, 1968, **49**, 1967-1968.
46. C. L. Braun, *The Journal of Chemical Physics*, 1984, **80**, 4157-4161.
47. P. J. Melz, *The Journal of Chemical Physics*, 1972, **57**, 1694-1699.
48. P. Peumans and S. R. Forrest, *Chemical Physics Letters*, 2004, **398**, 27-31.
49. A. Grunnet-Jepsen, D. Wright, B. Smith, M. S. Bratcher, M. S. DeClue, J. S. Siegel and W. E. Moerner, *Chemical Physics Letters*, 1998, **291**, 553-561.
50. J. A. Herlocker, C. Fuentes-Hernandez, K. B. Ferrio, E. Hendrickx, P. A. Blanche, N. Peyghambarian, B. Kippelen, Y. Zhang, J. F. Wang and S. R. Marder, *Applied Physics Letters*, 2000, **77**, 2292-2294.
51. Y. Pochi, *Quantum Electronics, IEEE Journal of*, 1989, **25**, 484-519.
52. M. H. Garrett, J. Y. Chang, H. P. Jenssen and C. Warde, *J. Opt. Soc. Am. B*, 1992, **9**, 1407-1415.
53. A. Grunnet-Jepsen, C. L. Thompson and W. E. Moerner, *J. Opt. Soc. Am. B*, 1998, **15**, 905-913.
54. C. W. Christenson, P.-A. Blanche, S. Tay, R. Voorakaranam, T. Gu, W. Lin, P. Wang, M. Yamamoto, J. Thomas, R. A. Norwood and N. Peyghambarian, *J. Display Technol.*, 2010, **6**, 510-516.
55. F. Bonaccorso, Z. Sun, T. Hasan and A. C. Ferrari, *Nat Photon*, 2010, **4**, 611-622.
56. Z. Liu, D. He, Y. Wang, H. Wu and J. Wang, *Synthetic Metals*, 2010, **160**, 1036-1039.
57. Z. Liu, Q. Liu, Y. Huang, Y. Ma, S. Yin, X. Zhang, W. Sun and Y. Chen, *Advanced Materials*, 2008, **20**, 3924-3930.
58. Q.-H. Wu, G. Hong, T. W. Ng and S. T. Lee, *Applied Physics Letters*, 2012, **100**, 161603-161604.
59. Q. Liu, Z. Liu, X. Zhang, L. Yang, N. Zhang, G. Pan, S. Yin, Y. Chen and J. Wei, *Advanced Functional Materials*, 2009, **19**, 894-904.
60. J. R. Potts, D. R. Dreyer, C. W. Bielawski and R. S. Ruoff, *Polymer*, 2011, **52**, 5-25.
61. P. Blake, P. D. Brimicombe, R. R. Nair, T. J. Booth, D. Jiang, F. Schedin, L. A. Ponomarenko, S. V. Morozov, H. F. Gleeson, E. W. Hill, A. K. Geim and K. S. Novoselov, *Nano Letters*, 2008, **8**, 1704-1708.
62. Y. Hernandez, V. Nicolosi, M. Lotya, F. M. Blighe, Z. Sun, S. De, I. T. McGovern, B. Holland, M. Byrne, Y. K. Gun'Ko, J. J. Boland, P. Niraj, G. Duesberg, S. Krishnamurthy, R. Goodhue, J. Hutchison, V. Scardaci, A. C. Ferrari and J. N. Coleman, *Nat Nano*, 2008, **3**, 563-568.